



# Green synthesis of iron oxide nanoparticles derived from water and methanol extract of *Centaurea solstitialis* leaves and tested for antimicrobial activity and dye decolorization capability

Zelal Isik<sup>a</sup>, Raouf Bouchareb<sup>b</sup>, Hudaverdi Arslan<sup>a</sup>, Sadin Özdemir<sup>c</sup>, Serpil Gonca<sup>d</sup>, Nadir Dizge<sup>a,\*\*</sup>, Deepanraj Balakrishnan<sup>e,\*</sup>, Sista Venkata Surya Prasad<sup>f,\*\*\*</sup>

<sup>a</sup> Department of Environmental Engineering, Mersin University, Mersin, 33343, Turkey

<sup>b</sup> Department of Environmental Engineering, Process Engineering Faculty, Saleh Boubnider University, Constantine, 25000, Algeria

<sup>c</sup> Food Processing Programme, Technical Science Vocational School, Mersin University, Mersin, 33343, Turkey

<sup>d</sup> Department of Pharmaceutical Microbiology, Faculty of Pharmacy, University of Mersin, Mersin, 33343, Turkey

<sup>e</sup> College of Engineering, Prince Mohammad Bin Fahd University, Al Khobar, 31952, Saudi Arabia

<sup>f</sup> Department of Electronics and Communication Engineering, MLR Institute of Technology, Hyderabad, 500043, India

## ARTICLE INFO

### Keywords:

Iron oxide nanoparticles  
Antimicrobial photodynamic activity  
Biofilm inhibition  
DNA cleavage  
Dyes removal  
Fenton reaction

## ABSTRACT

In this research, nanoparticles derived from water extract of *Centaurea solstitialis* leaves were used as green adsorbent in Fenton reaction for Reactive Red 180 (RR180) and Basic Red 18 (BR18) dyes removal. At optimum operating conditions, nanoparticles proved high performance in the tested dyes removal with more than 98% of removal elimination. The free-radical scavenging, DNA nuclease, biofilm inhibition capability, antimicrobial activity, microbial cell viability, and antimicrobial photodynamic therapy activities of the iron oxide nanoparticles (FeO-NPs) derived from water and methanol extract of plant were investigated. Each of the following analysis: SEM-EDX, XRD, and Zeta potential was implemented for the prepared NPs characterization and to describe their morphology, composition and its behavior in an aqueous solution, respectively. It was found that, the DPPH scavenging activities increased when the amount of nanoparticles increased. The highest radical scavenging activity achieved with FeO-NPs derived from water extract of plant as 97.41% at 200 mg/L. The new green synthesized FeO-NPs demonstrated good DNA cleavage activity. FeO-NPs showed good *in vitro* antimicrobial activities against human pathogens. The results showed that both synthesized FeO-NPs displayed 100% antimicrobial photodynamic therapy activity after LED irradiation. The water extract of FeO-NPs and methanol extract of FeO-NPs also showed a significant biofilm inhibition.

## 1. Introduction

Turkey is one of the world's richest countries in terms of floristics and herbal variety, with a flora that includes approximately 12,000 vascular plants used in a variety of disciplines such as medicine, engineering, chemistry, and so on (Alper et al., 2021). *Centaurea solstitialis* (Cs) is a member of the Asteraceae family and it is known as yellow star thistle or goblin thistle. Although Cs grows mainly in the Mediterranean region, it can be found on all six continents (Hierro et al., 2009; Dukes JS et al., 2013). It is an annual herbaceous plant that grows up to 60 cm with yellow or pink flowers. It is a durable plant due to its long roots and

due to the ability of its seeds to withstand fire. The plant is found in pine forests, dry slopes, fallow fields, and waste areas (Alper et al., 2021; Klahan et al., 2023). Cs, on the other hand, is an invasive and highly effective plant in terms of ecology. They are well-known for their toxic and harmful effects on other species (Eskikaya et al., 2022; Khan et al., 2023; Lu-Irving et al., 2019). In this regard, they are generally unappealing and economically insignificant plants. It has previously been used to treat herpes infections around the lips, malaria, nausea, cold, hemorrhoids, peptic ulcers, and abdominal pain (Yeşilada et al., 1995; Yilmaz, 2018; Alper and Güneş, 2019). Cs may be a prominent alternative raw material for green synthesis production in this context, owing

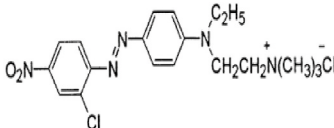
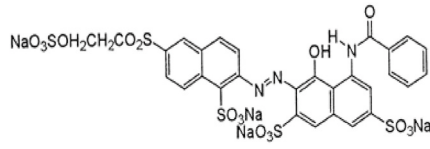
\* Corresponding author.

\*\* Corresponding author.

\*\*\* Corresponding author.

E-mail addresses: [nadirdizge@gmail.com](mailto:nadirdizge@gmail.com) (N. Dizge), [babudeepan@gmail.com](mailto:babudeepan@gmail.com) (D. Balakrishnan), [prasad.sista@gmail.com](mailto:prasad.sista@gmail.com) (S.V.S. Prasad).

**Table 1**  
The studied dyes chemical structures and fundamental properties.

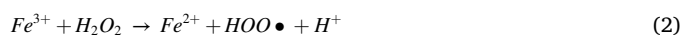
Dye	Basic Red 18 (BR18)	Reactive Red 180 (RR 180)
<b>Chemical Structure</b>		
<b>Molecular Classification</b>	Mono-azo class	Single-azo class
<b>Molecular Formula</b>	C <sub>19</sub> H <sub>25</sub> N <sub>5</sub> Cl <sub>2</sub> O <sub>2</sub>	C <sub>29</sub> H <sub>19</sub> N <sub>3</sub> Na <sub>4</sub> O <sub>17</sub> S <sub>5</sub>
<b>Molecular Weight(g/mol)</b>	426.34	933.76
<b>UV absorption λ<sub>max</sub> (nm)</b>	484	542

to its extensive availability and low-cost effectiveness.

Nanotechnology is a division of science which is concerned with the design, characterization, and manufacture of 1–100 nm particles at the atomic and molecular levels (Ensafi et al., 2010; Raouf et al., 2011; Karaman et al., 2021). In the last few decades, there has been an increase in interest in nanostructures due to nanotechnological works operating in all fields of life and new products that have been improved by incorporating these constitutions into large material components and systems (Dreher, 2004; Eskikaya et al., 2022; Dave and Chopda, 2014).

Metal oxides have known a great importance in many areas such as chemistry, physics, materials science, biogas production and antibacterial activity (Taherkhani et al., 2014; Karimi-Maleh et al., 2014; Alavi-Tabari et al., 2018; Bhuyar et al., 2020; Jadhav et al., 2021; Bouchareb et al., 2022). Unlike bulk materials, metal NPs have distinct chemical, physical, electrical, electronic, thermal, magnetic, dielectric, catalytic, biological, and optical properties (Deokar and Ingale, 2016; Mishra et al., 2022; Pandey et al., 2022). Iron oxide NPs have diverse polymorph ( $\alpha$ -Fe<sub>2</sub>O<sub>3</sub>,  $\gamma$ -Fe<sub>2</sub>O<sub>3</sub>, FeO and Fe<sub>3</sub>O<sub>4</sub>) structures (Kumar et al., 2020). In addition to all metal NPs, FeO-NPs have been broadly studied in areas such as sensors, photocatalysts, plant growth regulators, fine ceramics, water treatment, data storage materials, medical applications, pigments, photoelectrochemical cells and anticorrosive chemicals (Rostamizadeh et al., 2020; Lee and Lee, 2010).

Fenton oxidation is an oxidation process that uses H<sub>2</sub>O<sub>2</sub> and soluble Fe<sup>2+</sup> or a solid Fe catalyst to produce hydroxyl radicals ( $\bullet$ OH) with a high oxidation potential (Lee and Lee, 2010). Organic compounds can be destroyed using Fenton's reagent. H<sub>2</sub>O<sub>2</sub> oxidizes Fe<sup>2+</sup> to Fe<sup>3+</sup>, forming a hydroxide ion and a hydroxyl radical in the process. Fe<sup>3+</sup> ion is then reduced to Fe<sup>2+</sup> by a different hydrogen peroxide molecule, resulting in the development of a proton and a hydroperoxyl radical. The disproportionation of hydrogen peroxide outcomes to the formation of two distinct oxygen-radical species as described in the following reactions (Eqs. (1)–(3)), with water as a byproduct (Behin et al., 2017).



This process produces free radicals, which are then used in subsequent reactions. The hydroxyl radical, for example, is a potent, non-selective oxidant (Cai et al., 2021). Organic compound oxidation by Fenton's reagent is exothermic and rapid, resulting in the contaminants oxidation to primarily CO<sub>2</sub> and H<sub>2</sub>O. In the 1930s, Haber and Weiss proposed reaction (1) as part of the Haber–Weiss reaction (Haber and Weiss, 1932). As an iron catalyst, iron (II) sulfate is commonly used. The

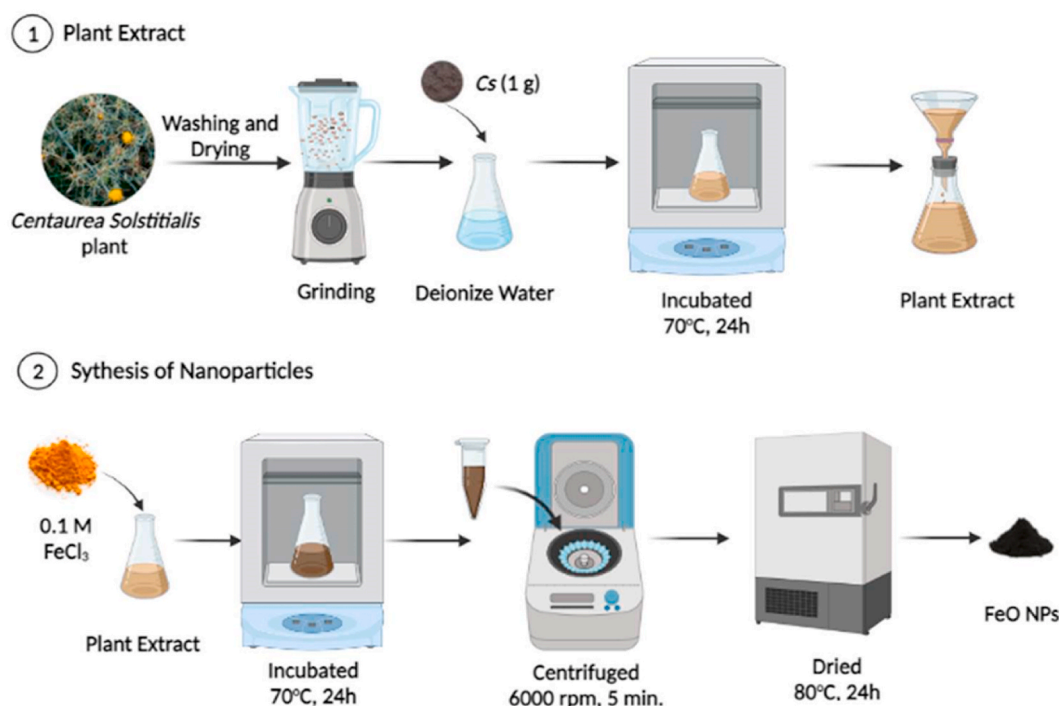


**Fig. 1.** FeO-NPs synthesis schematic representation.

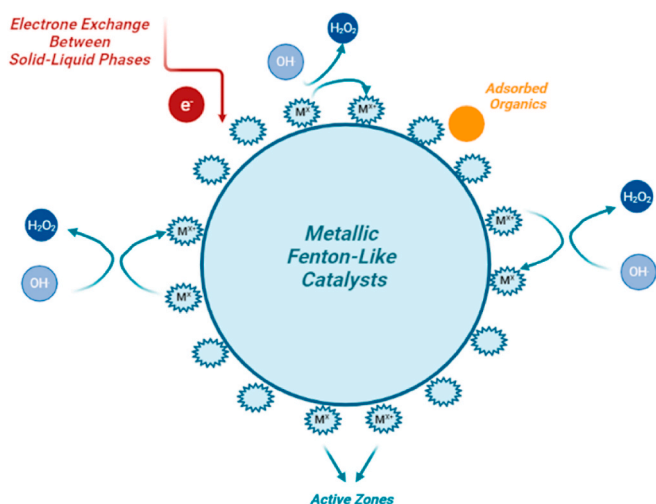


Fig. 2. Fenton-like process reaction mechanism.

exact redox cycle mechanisms are unknown, and non-OH<sup>•</sup> oxidizing organic compound mechanisms have been proposed as well (Sheldon and Kochi, 1976). As a result, rather than focusing on a specific Fenton reaction, discussing Fenton chemistry in general may be more appropriate.

In this research, we aimed to synthesize iron oxide nanoparticles (FeO-NPs) using *Centaurea solstitialis* (Cs) leaf extract. The synthesized FeO-NPs from the Cs (a harmful plant and no economic values) which may serve as a new and alternative raw material for green synthesis production. The synthesized nanoparticles from different plant extracts were characterized and used as adsorbent in Fenton reaction for Reactive Red 180 (RR180) and Basic Red 18 (BR18) dyes removal. In addition, DPPH scavenging activity, biofilm inhibition capability, antibacterial activity, microbial cell viability inhibition, and FeO-NPs antimicrobial photodynamic therapy were examined.

## 2. Materials and methods

### 2.1. Materials and chemicals

The following used chemicals: synthetic dyes (Basic Red 18, Reactive Red 180), iron (III) chloride (FeCl<sub>3</sub>), sodium hydroxide (NaOH), hydrochloric acid (HCl), and hydrogen peroxide (H<sub>2</sub>O<sub>2</sub>) were brought from Sigma Aldrich. FeCl<sub>3</sub> was used as the iron source. The molecular structures and basic properties of the used dyes are shown in Table 1.

Cs was collected from Mersin, Turkey. Cs was cleaned with deionized water several times. The cleaned leaves were dried in the air and then ground to fine powder which was stored at room temperature for further usage.

### 2.2. Synthesis of FeO-NPs

Cs extract was prepared as follows: 1 g CsP was added into 250 mL of deionize water and agitated 24 h at 70 °C. As the next step, the extract has been filtered through a funnel to obtain the final solution. 0.1 M FeCl<sub>3</sub> solution (100 mL) is prepared with the obtained plant extract. The mixture was incubated in an oven at 70 °C for 24 h. Then, the mixture was centrifuged at 6000 rpm for 5 min. The obtained deposit solid was separated and used as FeO-NPs in the Fenton experiments. All the followed experimental steps are demonstrated in Fig. 1.

### 2.3. FeO-NPs characterization

SEM–EDX was elaborated to characterize the synthesized nanoparticles. Scanning electron microscopy (SEM) (SEM, Zeiss Supra 55,

Germany) was used to determine the surface morphology of nanoparticles. In addition, the composition of the elements present on the nanoparticles' surface was carried out using energy dispersive X-ray spectroscopy (EDX). XRD measurements were carried out using via X-ray diffraction device (XRD, Bruker, D8 Venture) with 2θ scan range from 10 to 90° at a scan rate of 2°/min. The zeta potential of nanoparticles was measured using a zeta sizer (Malvern Zetasizer equipped with MPT-2 Titrator, Nano ZS).

### 2.4. Fenton experiments

The Fenton-like experiments of FeO-NPs were established in conical flasks comprising 50 mL of dye solution. All the experiments were elaborated under constant conditions: shaking speed of 150 rpm for 60 min at 25 ± 1 °C. Then, the dye solutions were centrifuged (6000 rpm and 5 min). Dyes concentrations (BR18 and RR180) were determined using UV–Vis spectrophotometer at determined wavelengths. The Fenton-like process reaction mechanism is illustrated in Fig. 2 (Hussain et al., 2021).

The effects of pH, concentration of nanoparticles and concentration of H<sub>2</sub>O<sub>2</sub> on the removing of dyes were investigated. Initially, pH effect on the removability of the studied dyes was evaluated as follows. The dyes pH was adjusted with dilute hydrochloric acid (HCl 0.1 M) to 2.0, 2.5, 3.0, 4.0, and 5.0. Then, 250 mg/L FeO-NPs and 5 μL hydrogen peroxide were added to each solution and agitated.

The impact of FeO-NPs amount and H<sub>2</sub>O<sub>2</sub> concentration on the removing of dyes were studied. Dyes pH was adjusted with 0.1 M NaOH and 0.1 M HCl. Different concentrations of FeO-NPs (125, 250, 375, and 500 mg/L) were added to the conical bottles containing 100 mg/L dye concentration and agitated.

In the effect of H<sub>2</sub>O<sub>2</sub> concentration investigation, diverse concentrations of H<sub>2</sub>O<sub>2</sub> (2.5, 5.0, 7.5, 10 μL/L) were added to the dye solutions. The concentration of BR18 and RR180 dyes were calculated using Eq. (4).

$$\text{Removal Efficiency (\%)} = \left( \frac{\text{Initial Concentration} - \text{Final Concentration}}{\text{Initial Concentration}} \right) \times 100 \quad (4)$$

### 2.5. DPPH scavenging activity

The DPPH radical scavenging activity of the new synthesized FeO-NPs was measured using the assay reported by Ağirtaş et al. (Ağirtaş et al., 2015). A 200 μL various concentration of FeO-NPs solutions prepared and added to the tubes. Later, 1.0 mL of DPPH was added to each tube and the total tubes were incubated at room temperature for 30 min. As control agents, Trolox and Ascorbic Acid were used. Methanol was used as blank. After 30 min, the purple color removal was measured at 517 nm under. The scavenging capability was computed using Eq. (5).

$$\text{Capacity (\%)} = \left( \frac{\text{Abs (control)} - \text{Abs (sample)}}{\text{Abs (control)}} \right) \times 100 \quad (5)$$

Abs<sub>control</sub>: control absorbance, Abs<sub>sample</sub>: the absorbance of the test compounds and DPPH.

### 2.6. DNA cleavage ability

The DNA cleavage ability of the synthesized FeO-NPs were conducted by agarose gel electrophoresis. Various concentrations of the green synthesized nanoparticles were mixed with the plasmid DNA (*E. coli* pBR 322) and the mixtures incubated at 37 °C for 1 h. Later, the mixtures were put into the wells of agarose gel. Then, electrophoresis assay started. Supercoiled plasmid DNA which was untreated was used as -ve control. A transilluminator was used to check DNA bands.

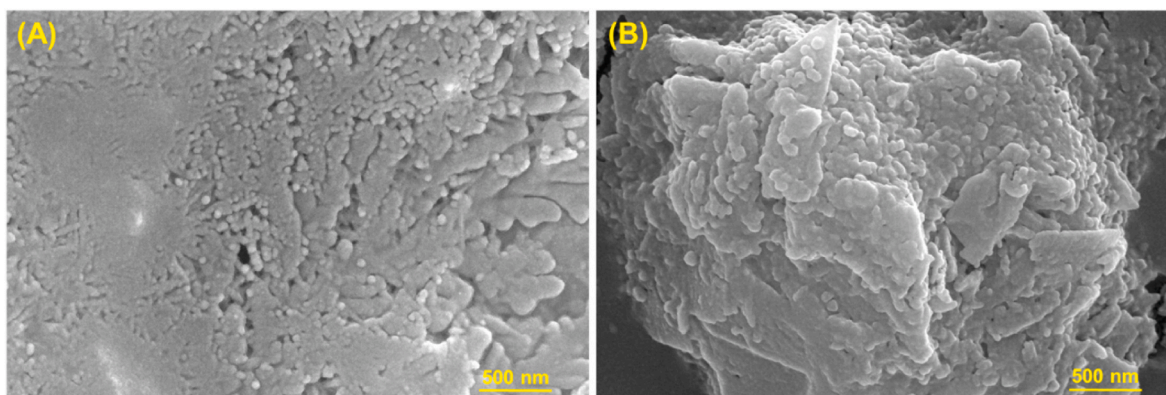


Fig. 3. SEM of FeO-NPs derived from (A) water and (B) methanol using *Cs* leaves.

2.7. Antimicrobial activity

Micro-dilution assay was employed to test the antimicrobial property of the green synthesized FeO-NPs. Gr + ve, Gr -ve and fungal strains including *E. faecalis*, *S. aureus*, *E. hirae*, *E. coli*, *P. aeruginosa*, *L. pneumophila*, *C. parapsilosis*, and *C. tropicalis* were used in the antimicrobial activity study. The ATTC numbers of the strains used, and the details of the antimicrobial study are given in our previous study (Gonca et al., 2021). Firstly, the nanoparticles were made two-fold (1:2) serial dilutions and they were incubated at 37 °C for 24 h with the aforementioned microorganisms (0.5 McFarland). Next, MIC was appraised to determine antimicrobial activity which showed the lowest concentration that inhibits microbial growth.

2.8. Cell viability and antimicrobial photodynamic therapy

*E. coli* was utilized as a bacterium to evaluate the cell viability inhibition capabilities of the green synthesized FeO-NPs. The cell viability inhibition method was carried out as mentioned in our previous study (Bautista et al., 2007). *E. coli* was inoculated to NB medium. Then, it was incubated at 37 °C and 150 rpm for 24 h. After centrifuging *E. coli*, the microbial pellet was cleaned with 0.9 percent sterile saline solution. *E. coli* was suspended in sterile saline solution. This bacterial solution was utilized to cell viability ability. *E. coli* was treated with the green synthesized FeO-NPs at different concentrations 125, 250, and 500 mg/L for 90 min at 37 °C. Later, the mixtures were diluted in different proportions and inoculated in NB agar and left to incubate at 37 °C for one day. The same procedure was also conducted for antibacterial photodynamic therapy study, after the compounds were subjected to LED light for 20 min. Finally, counting the formed colonies was elaborated, and

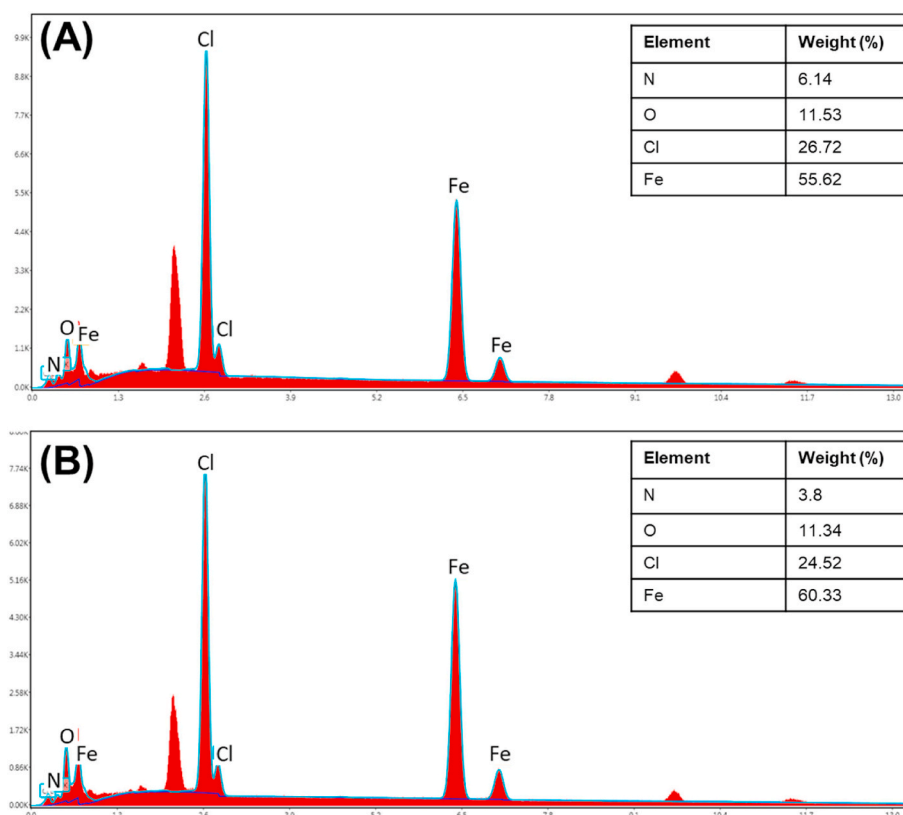


Fig. 4. EDX of FeO-NPs derived from (A) water and (B) methanol using *Cs* leaves.

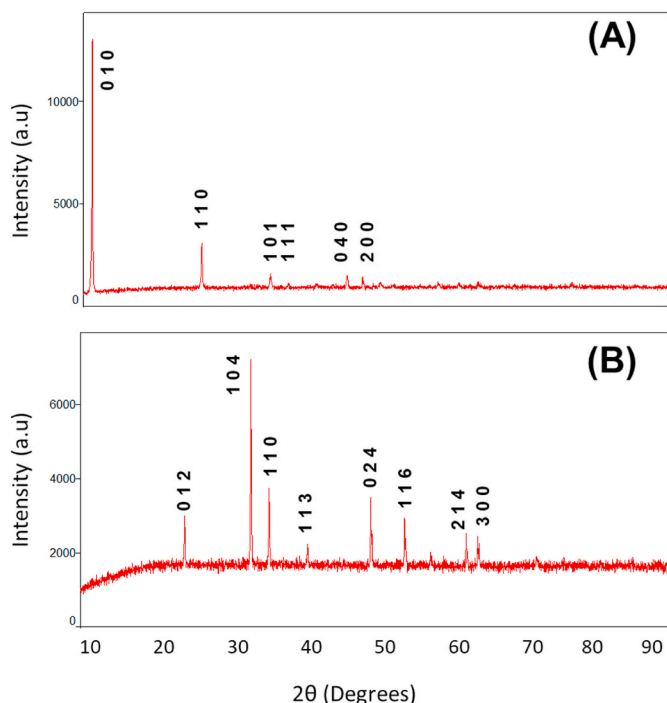


Fig. 5. XRD of FeONPs derived from (A) water and (B) methanol using Cs leaves.

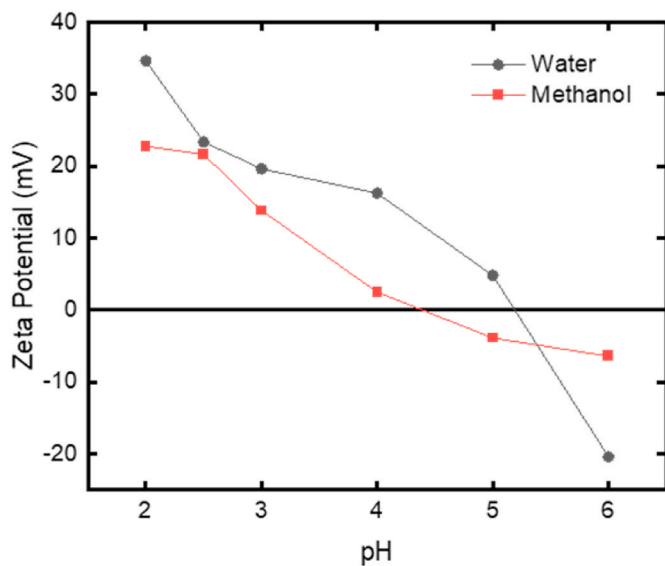


Fig. 6. Zeta potential values of the nanoparticles.

the cell viability was computed using Equation (6).

$$\text{Cell viability (\%)} = \left( \frac{A(\text{control}) - A(\text{sample})}{A(\text{control})} \right) \times 100 \quad (6)$$

### 2.9. Biofilm inhibition activity

The biofilm formation inhibition capability of the FeO-NPs was studied based upon crystal violet (CV) staining. Two selected bacteria (*P. aeruginosa* and *S. aureus*) were utilized to appraise the biofilm inhibition of the green synthesized FeO-NPs. One night before starting the testing step, bacterium cultures were grown. Bacterial strains were inoculated to well plates with  $2.9 \times 10^8$  CFU/mL. Bacterial strains

incubated at 37 °C for 72 h in well plates containing different levels of FeO-NPs at 125, 250, and 500 mg/L. Following, the wells were drained and cleaned. The plates were dried in the oven. Next, CV was added into the well. CV removed after 45 min and the plates were washed slowly. The washing step was done twice. Ethanol was then added and waited 15 min for the absorbed CV to be recovered. Absorbance of solutions was measured at 595 nm wavelength. Wells used as positive control did not contain nanoparticles but only bacteria. Biofilm inhibition was calculated according to Eq. (7).

$$\text{Biofilm Inhibition (\%)} = \left( \frac{\text{Abs}(\text{control}) - \text{Abs}(\text{sample})}{\text{Abs}(\text{control})} \right) \times 100 \quad (7)$$

## 3. Results and discussion

### 3.1. FeO-NPs characterization

Both FeO-NPs derived from water and methanol extract of Cs leaves were characterized in terms of SEM-EDX, XRD, and ZETA POTENTIAL as represented in Figs. 3–6. Fig. 3 shows the surface morphology of the synthesized nanoparticles. As evident from SEM images, nanoparticles derived from water (Fig. 3A) exhibited perfect homogeneous spherical morphology compared to the different inhomogeneous morphology shown in Fig. 3B corresponding to nanoparticles derived from methanol. Therefore, Fenton experiments were conducted using iron oxide nanoparticles derived from water extract of Cs leaves.

Elemental composition of the nanoparticles was studied with EDX. Fig. 4A and B show the EDX analysis of the Fe<sub>2</sub>O<sub>3</sub> NPs derived from water and methanol, respectively. As evident from Fig. 4A, the expected elements N (6.14% w/w), O (11.53% w/w), Cl (26.72% w/w), and Fe (55.62% w/w) are observed clearly and in an appropriate proportion. Similar proportions were obtained when prepared NPs were derived from methanol as shown in Fig. 4B: N (3.8% w/w), O (11.34% w/w), Cl (24.52% w/w), and Fe (60.33% w/w).

X-ray diffraction (XRD) spectroscopy was used to investigate the crystalline structure of the prepared NPs as shown in Fig. 5. The diffraction pattern of the sample derived from water (Fig. 5A) has extremely broad line widths due to its small uniform size. However, there are still-detectable sharp peaks situated on the diffraction angles 2θ value of 10° and 110°.

Fig. 6 Depicts the change in zeta potential as a function of pH from 2 to 6. NaCl (1 mM) was used to make the solutions. When the zeta potential of the nanoparticles was investigated, it was observed that the zeta potential of the nanoparticles produced in pure water was almost positively charged for all pH values except of pH 6. However, the nanoparticles produced in methanol were positively charged between pH 2–4. They were charged negatively beyond at this pH. As a result, the adsorption capacity of the nanoparticles decreased for anionic dyes below pH 4.

### 3.2. Fenton experiments

In this research, the potential of iron oxide nanoparticles derived from water of Cs plant for RR180 and BR18 dyes removal in Fenton reaction was investigated. In this process, pH is most likely the most important control parameter. Although the Fenton reaction has been shown to have high removal efficiencies for a variety of pollutants, most studies have been conducted at acidic pH. (Bautista et al., 2007; Baycan and Can, 2019; El-Desoky et al., 2010). pH of the aqueous solution has been stated to have an important effect on the dye molecules adsorptive uptake due to its influence on both the dye molecule ionization process and the binding-sites of adsorbent surface (Sathishkumar et al., 2012). Initially, Fenton reaction was studied for RR180 and BR18 dyes removal at various solution pH conditions, and the experimental results are shown in Fig. 7A. Concentration of dyes, H<sub>2</sub>O<sub>2</sub> concentration and adsorbent amount were kept constant: 100 ppm, 5 μL/L, and 0.25 g/L,

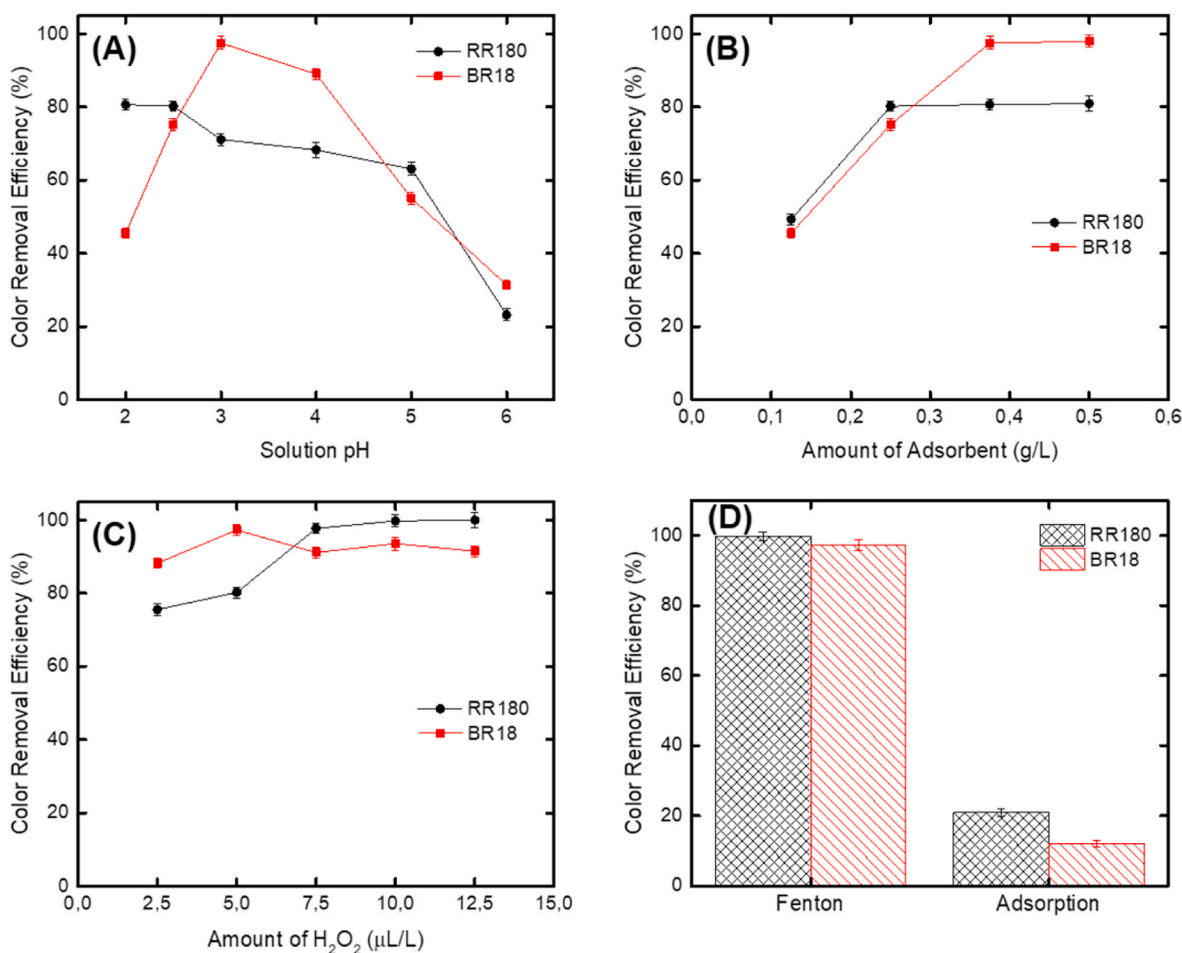


**Fig. 7.** The optimization of parameters for Fenton experiments using iron oxide nanoparticles derived from water (Experimental conditions: (A) Dye concentration: 100 ppm; amount of adsorbent: 0.25 g/L; amount of H<sub>2</sub>O<sub>2</sub>: 5 μL/L; time: 60 min. (B) Dye concentration: 100 ppm; solution pH: 2.5 for RR180 and 3.0 for BR18; amount of H<sub>2</sub>O<sub>2</sub>: 5 μL/L; time: 60 min. (C) Dye concentration: 100 ppm; amount of adsorbent: 0.25 g/L; solution pH: 2.5 for RR180 and 3.0 for BR18; time: 60 min. (D) Similar Fenton and adsorption processes operating conditions of dye concentration: 100 ppm; amount of adsorbent: 0.25 g/L; solution pH: 2.5 for RR180 and 3.0 for BR18; time: 60 min. Fenton reaction conducted for H<sub>2</sub>O<sub>2</sub> amount of 10 μL/L for RR180 and 5 μL/L for BR18.

respectively. As shown in Fig. 7A, the RR180 removal efficiencies were 80%, 80%, 70%, 67%, 62%, and 20% at pH 2, 2.5, 3, 4, 5, and 6, respectively, with subsequent BR18 color elimination of 43%, 77%, 98%, 89%, 57%, and 31% at pH 2, 2.5, 3, 4, 5, and 6, respectively. RR180 and BR18 dyes adsorption was maximum at pH 2.5 and pH 3, respectively. As solution pH increased, RR180 dye removal decreased continuously in the studied pH range. In the other hand, BR18 removal has known a better removal performance at pH value of 3.0. Similar compartment was replicated for the removal of several textile dyes on different adsorbents (Sathishkumar et al., 2012; Raji et al., 2021; Yang et al., 2018). The electrical charge of the adsorbent surface and the ionic structures of the dye in solution vary in function of solution pH (Sathishkumar et al., 2012). Hence, the ionization conditions of the functional groups on both adsorbent surface and dye molecule influence the degree of interaction between the dye and adsorbent (Gusain et al., 2020). The best dyes removal at acidic pH can be accredited to the electrostatic interactions between the adsorbent and the investigated adsorbates (RR180 and BR18 dyes). At acidic pH, more hydroxyl radicals are formed in Fenton reaction; consequently, resulting in more dye elimination. At higher pH, iron hydroxides precipitation could inhibit the ferrous ions regeneration resulting hydroxyl groups (OH<sup>•</sup>) generation for further oxidation (El-Desoky et al., 2010; Sathishkumar et al., 2012; Raji et al., 2021). The differences in dyes elimination performances achieved for acidic pH and pH 6 reflect the importance of pH impact in Fenton reaction.

Adsorbent concentration is another key parameter for the Fenton reaction since this may reduce the adsorbent capacity for a particular dye content (Sathishkumar et al., 2012). The results of Fenton reaction in function of adsorbent amount for RR180 and BR18 dyes elimination at optimum pH values 2.5 and 3, respectively, are shown in Fig. 7B. As adsorbent concentration increased from 0.25 g/L to 0.5 g/L, both dyes removal efficiencies were not enhanced compared to the results illustrated in Fig. 7A. When lower adsorbent amount (0.125 g/L) was used, poor removal efficiency of less than 50% was registered for both tested dyes. When adsorbent concentration increases, iron concentration leached in the aqueous solution increases resulting in an enhancement of oxidation effectiveness and eventually better dye removal takes place (Yang et al., 2018). When excessive adsorbent quantity was used (more than 0.25 g/L), the oxidation activity of the catalyst did not enhance as shown in Fig. 7B. Hence, further experiments of Fenton reaction for RR180 and BR18 dyes removal were conducted with the adsorbent concentration of 0.25 g/L.

As the treatment method cost is a viable factor, H<sub>2</sub>O<sub>2</sub> concentration optimization is crucial in wastewater treatment using Fenton reaction. Fig. 7C displays RR180 and BR18 decolorization in function of H<sub>2</sub>O<sub>2</sub> concentration in the range of 2.5 μL/L and 12.5 μL/L at optimal operating conditions of pH and adsorbent concentration for each studied dye. As shown in Fig. 7C, when H<sub>2</sub>O<sub>2</sub> concentration was increased, RR180 removal efficiency has increased from 77% up to nearly complete elimination for 10 μL/L of H<sub>2</sub>O<sub>2</sub> concentration showing one positive

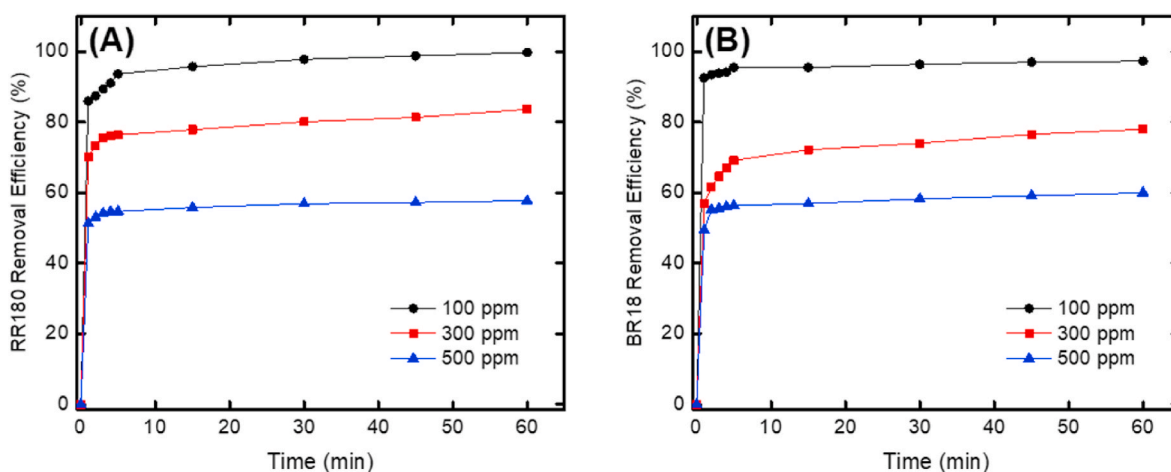


**Fig. 8.** Dye concentration effect on Fenton experiments using iron oxide nanoparticles derived from water (Experimental conditions: Amount of adsorbent: 0.25 g/L; solution pH: 2.5 for RR180 and 3.0 for BR18; amount of  $H_2O_2$ : 10  $\mu$ L/L for RR180 and 5  $\mu$ L/L for BR18; time: 60 min.

significant color removal for all the studied  $H_2O_2$  concentration. Contrarily for BR18 dye removal, the elimination process for all studied  $H_2O_2$  concentrations can be classified into two areas, namely a positive significant color elimination in the range between 2.5  $\mu$ L/L and 5.0  $\mu$ L/L, followed by a negative oxidation rate. The best removal efficiency was obtained for only 5  $\mu$ L/L of  $H_2O_2$  concentration corresponding to 98% of BR18 dye elimination. However, further increase of  $H_2O_2$  concentration from 5.0  $\mu$ L/L to 12.5  $\mu$ L/L has slightly decreased color removal rate. The lower performance of color removal obtained with 2.5  $\mu$ L/L  $H_2O_2$  indicates an insufficient number of hydroxyl radicals for the treatment of 100 ppm concentration of the synthetic dye wastewater. As stated in previous research (Bautista et al., 2007; Baycan and Can, 2019), stoichiometric weight ratio of  $H_2O_2$  should be studied according to the treated water pollutants content. An excessive  $H_2O_2$  concentration leads to a decreased efficiency of colors removal compared to what was obtained with 5.0  $\mu$ L/L  $H_2O_2$  at the case of BR18 in this study. This is because of the scavenging role of  $H_2O_2$  excess dosage, in which the formed hydroxyl radicals react with hydrogen peroxide instead of being consumed by dyes molecules (Baycan and Can, 2019; El-Desoky et al., 2010; Sathishkumar et al., 2012; Raji et al., 2021). Fig. 7D illustrates a comparison between Fenton reaction and adsorption processes for RR180 and BR18 dyes removal at the same operating conditions of dye concentration 100 ppm, adsorbent concentration 0.25 g/L, solution pH: 2.5 for RR180 and 3.0 for BR18 and reaction time of 60 min. From Fig. 7D, the impact of Fenton reaction is evident compared to the poor removal results obtained by just adsorption process, where both RR180 and BR18 dyes removal efficiencies were only 20% and 13%, respectively.

Fig. 8 illustrates the impact of the initial dye concentration on Fenton experiments using iron oxide nanoparticles derived from water at the following optimal experimental conditions: amount of adsorbent: 0.25 g/L; solution pH: 2.5 for RR180 and 3.0 for BR18; amount of  $H_2O_2$ : 10  $\mu$ L/L for RR180 and 5  $\mu$ L/L for BR18 and reaction time of 60 min. The following initial dyes concentrations (100, 300, and 500 ppm) were investigated. Fig. 8 Depicts the obtained results. As shown in Fig. 8, both dye removal processes for all initial dye concentrations are clearly classified into two distinctive regions, a rapid color removal during first 02 min, followed by a slowing down of the removal rate. The fast adsorption rate during the first 02 min designates the importance of the specific surface on the adsorption process. The obtained results indicate that the elimination percentage of both dyes removal efficiencies decreased with the increase of initial dye concentration. The rate and the mechanism of a dye elimination depends on colors solubility and their chemical properties (Shen et al., 2001). For instance, after 60 min of reaction, RR180 dye removal (Fig. 8A) decreased from 99% to 57%, and

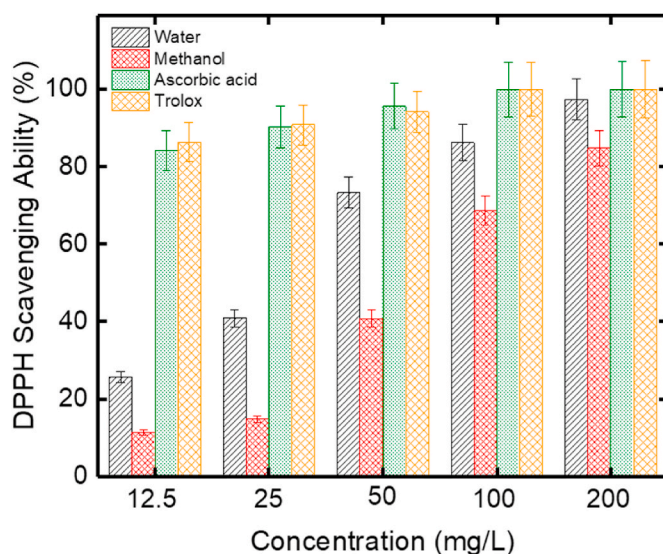


**Fig. 9.** DPPH scavenging ability of the synthesized green FeO-NPs. (For interpretation of the references to color in this figure legend, the reader is referred to the Web version of this article.)

BR 18 color removal (Fig. 8B) decreased from 98% to 60%, when initial dye concentration was augmented from 100 to 300 ppm. It can be credited to the saturation of the available adsorption sites on the adsorbent as the different dye solutions were subject to the same experimental conditions of adsorbent amount, pH,  $H_2O_2$  concentration and reaction time. Pelosi et al. (2014) stated that the removal efficiency of dye decreases when the initial color concentration increases concluding to the saturation at higher color concentrations (Pelosi et al., 2014).

### 3.3. Scavenging activity of DPPH radical

DPPH scavenging activity is the most used as antioxidant test procedure because it is a fast, simple, cheap, and effective method to determine the organic and inorganic compounds. The DPPH scavenging ability of the FeO-NPs derived from water and methanol extract of plant were studied at different concentrations ranges from 12.5 mg/L to 200 mg/L as illustrated in Fig. 9. The FeO-NPs derived from water extract of the plant showed higher antioxidant activity than the FeO-NPs derived from methanol extract for all tested concentrations. The DPPH

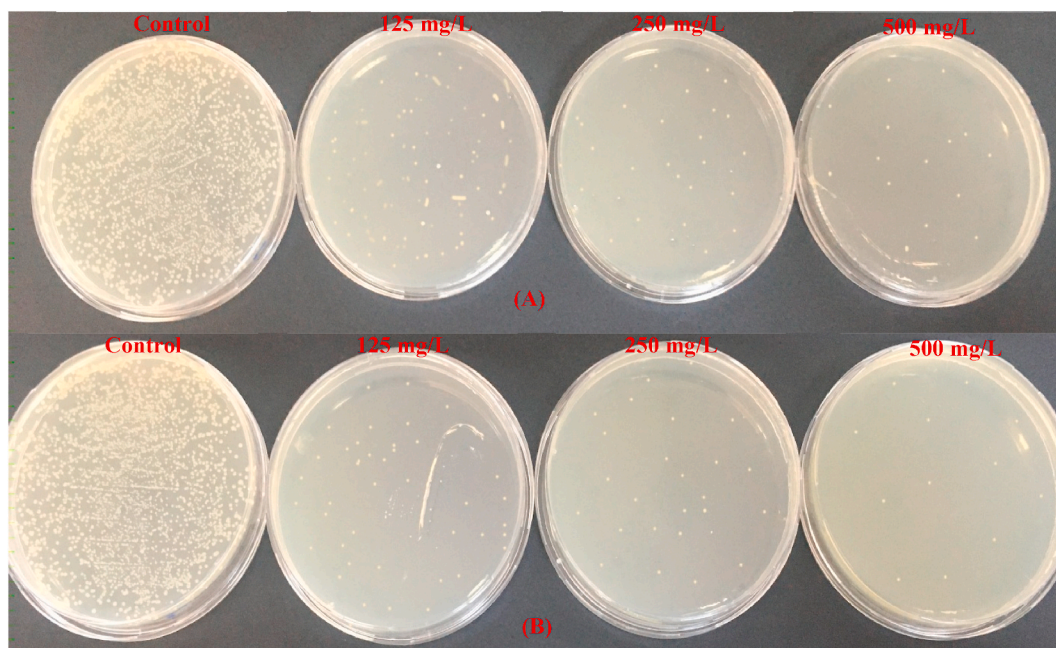


Fig. 10. Microbial cells in function of FeO-NPs concentration derived from (A) water extract and (B) methanol extract.

scavenging activity of the FeO-NPs derived from water and methanol extract of plant were (25.68% and 11.33%) at 12.5 mg/L, respectively and (86.22% and 68.72%) at 100 mg/L, respectively. In this research, the highest radical scavenging activity achieved with the FeO-NPs derived from water extract of plant as 97.41% at 200 mg/L. The result of antioxidants on DPPH can be attributed to their hydrogen donating ability (Chavan et al., 2020). Sandupatla et al. (2021) have investigated the antioxidant activity of Fe, Ag and Fe–Ag nanoparticles synthesized from *Passiflora edulis* by DPPH free radical scavenging process. They indicated that the FeO-NPs exhibited a percentage of radical scavenging ranges between 1.69% at 25 mg/L and 38.47% at 400 mg/L. Iqbal et al. (2020) described that the antioxidant activity of the green synthesized FeO-NPs derived from the *Rhamnella gilgitica* and the green synthesized FeO-NPs displayed strong radical scavenging ability and showed concentration depended on activity. The highest DPPH radical scavenging activity was found 78.36% at 2000 mg/L of concentration. Mirza et al.

(2018) synthesized and characterized FeO-NPs using *Agrewia optiva* and *Prunus persica* leaf extract. They also evaluated the antioxidant activity of both green synthesized iron oxide nanoparticles by DPPH scavenging activity and both green synthesized iron oxide nanoparticles demonstrated approximately 15%–40% radical scavenging activity. Results of this study showed that green synthesized FeO-NPs can be used as an antioxidant agent after conducting the following investigations.

### 3.4. DNA cleavage ability

DNA is the most important molecule in living organisms. A change in this molecule threatens the life of the living being. With this principle, DNA is one of the most important molecules targeted in anticancer and antimicrobial studies. When pBR322 plasmid DNA is subjected to agarose gel electrophoresis, fast migration is occurred for the Form I (supercoiled form). Depending on the cleavage abilities of the

Table 2

A comparison of our nanoparticles to previously published work.

Green materials	Iron Type	Environmental application	Antimicrobial & Antioxidant activations	Major findings	Reference
<i>Amla seeds</i>	Iron oxide nanoparticles	Methylene blue dye removal from water	-	80% of the Methylene blue was removed	Ashraf et al. (2022)
<i>Melia azedarach flowers</i>	Iron oxide nanoparticles	-	Antimicrobial and antioxidant activities	Comparatively less antioxidant activity than extract alone	Muzafar et al. (2022)
<i>Echinochloa frumentacea grains</i>	Iron oxide nanoparticles	-	Antimicrobial and antioxidant activities	95.10% Antioxidant activity	Velsankar et al. (2022)
<i>Azardica indica leaves</i>	Super paramagnetic iron oxide nanoparticles	Adsorption	-	83% dye removed	Getahun et al. (2022)
<i>Ziziphora clinopodioides lam leaf</i>	Iron nanoparticle	-	Antioxidant activities	In vitro field, FeNPs indicated the high antioxidant property against DPPH.	Chen et al. (2022)
<i>Cleistocalyx operculatus leaf</i>	Zero-valent iron nanoparticles	Removal of dye (rhodamine B)	-	95% of the rhodamine B was removed	Le et al. (2022)
<i>Canthium coromandelicum leaf</i>	Iron oxide nanoparticles	Photocatalytic oxidation (Janus green B)	Antibacterial and catalytic degradation	97.23% of the Janus green B was removed,	Sudhakar et al. (2021)
<i>Pheonix dactylifera leaf</i>	Iron nanoparticles	-	Antioxidant activity	50% DPPH antioxidant activity	Abdullah et al. (2020)
<i>Centauria solstitialis leaves</i>	Iron oxide nanoparticles	Fenton-like process,	Antimicrobial and biofilm inhibition activity	97.23% of the Reactive Red 180 and Basic Red 18 were removed, and 100% antimicrobial photodynamic therapy activity	This study



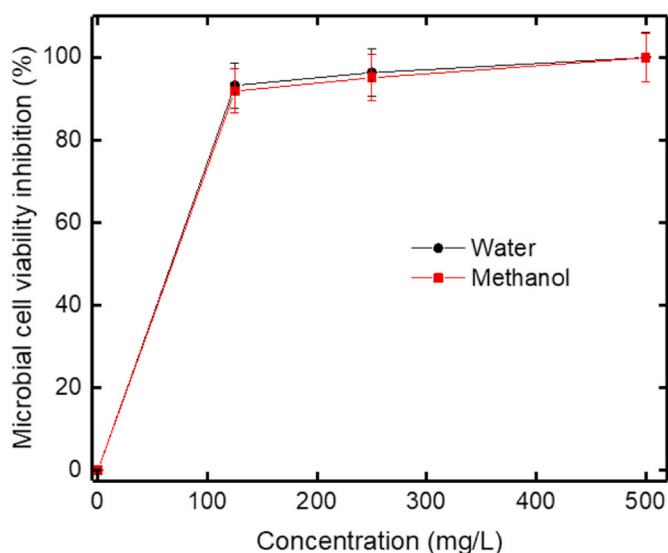


Fig. 11. Microbial cell viability inhibition in function of iron oxide nanoparticles concentration.

compounds, supercoiled form can convert to form II (nicked form), form III (linear form), or both (De et al., 2022; Vasseghian et al., 2022). Therefore, DNA targeting molecules are needed for antimicrobial and anticancer activity studies. In this research, DNA cleavage activity of synthesized FeO-NPs was tested. The results are displayed in Fig. 10. As illustrated in Fig. 10, it is observed that the FeO-NPs synthesized from the water extract completely fragmented the DNA molecule, while the FeO-NPs synthesized from the methanol extract caused single chain breaks. DNA cleavage activities of different metal nanoparticles were tested in different studies. Duman et al. (2016) investigated DNA nuclease activity of the CuO NPs derived from *Chamomile* flower extract on the plasmid pBR322 DNA and it was tested by gel electrophoresis

assay. They indicated that when pBR322 plasmid DNA reacted with the CuO-NPs derived from *Chamomile* flower extract, a single strain cleavage activity was observed. De et al. stated that new ZnO NPs were synthesized and characterized using *Syzygium aromaticum* bud extract. They also explored the DNA cleavage activity of ZnO NPs. These nanoparticles demonstrated DNA cleavage ability. Antonoglou et al. (2019) synthesized and characterized CuFeO<sub>2</sub>-NPs. They also studied the DNA cleavage activity of the new synthesized CuFeO<sub>2</sub>-NPs. It was found that CuFeO<sub>2</sub> did not show any DNA cleavage activity at 10 mg/L while it was displayed DNA cleavage activity at 50 and 100 mg/L concentrations. According to the obtained results in the present research, both synthesized FeO-NPs showed DNA cleavage activity and the FeO-NPs synthesized from water extract can be used in anticancer and antimicrobial studies after toxicological test studies.

### 3.5. Antimicrobial activity

Table 2 demonstrates the minimum inhibition concentrations (MICs) values of green synthesized FeO-NPs from water and methanol plant extracts. As shown in Table 2, the antimicrobial effect of green synthesized FeO-NPs was quite good. The MICs of FeO-NPs synthesized from methanol plant extract were determined *E. coli*, *P. aeruginosa*, *L. pneumophila*, and *C. parapsilosis* were 256 mg/L and 128 mg/L for *E. hirae*, *E. fecalis*, *S. aureus*, and *C. tropicalis*, respectively. According to these findings, *E. hirae* and *S. aureus* were the most sensitive bacteria to green FeO-NPs synthesized from plant water extract. The antimicrobial effect of green synthesis of Ag-Fe bimetallic NPs against Gram-negative *E. coli* and Gram-positive *S. aureus* was investigated by Al-Asfar et al. (2018) using disk diffusion assay. They indicated that when the concentration of bimetallic Ag-Fe-NPs raised the antimicrobial activity of Ag-Fe bimetallic NPs raised up against tested microorganisms. Yoon et al. (2020) informed that they studied the  $\alpha$ -Fe<sub>2</sub>O<sub>3</sub> nanoparticles antibacterial activity against *Streptococcus mutans*, *S. aureus*, *P. aeruginosa*, and *E. coli* and it was found that  $\alpha$ -Fe<sub>2</sub>O<sub>3</sub> nanoparticles demonstrated antimicrobial activity. Patra and Baek (2017) synthesized

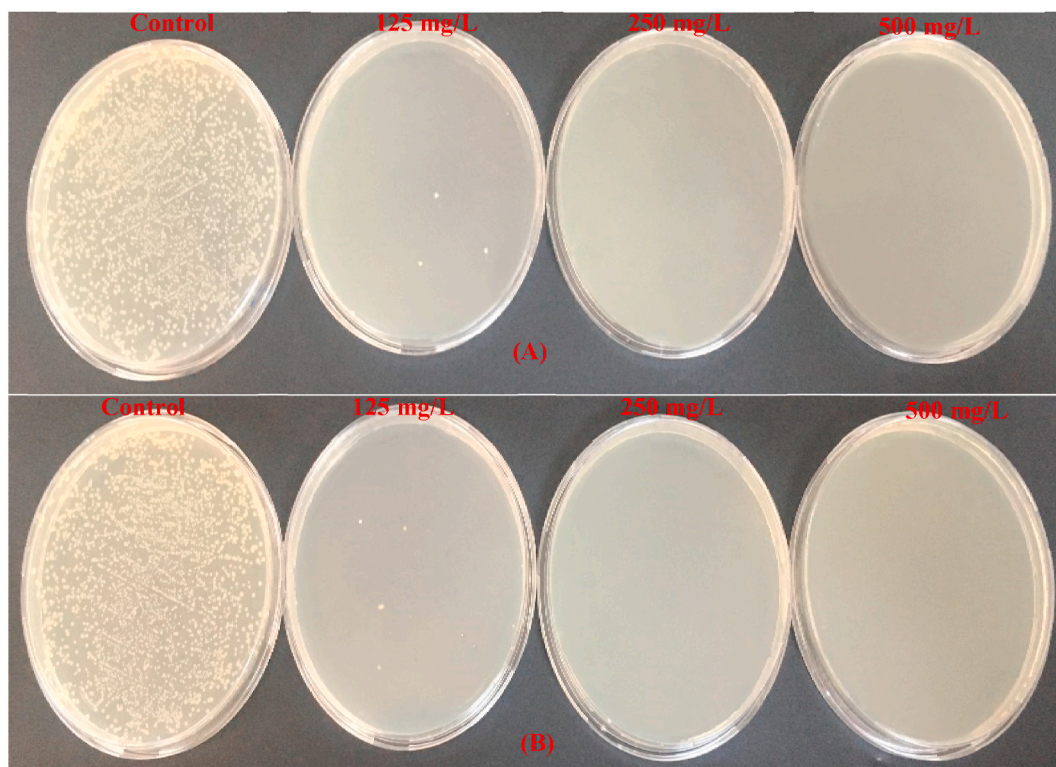


Fig. 12. Antimicrobial photodynamic activity cells in function of FeO-NPs concentration derived from (A) water extract and (B) methanol extract.

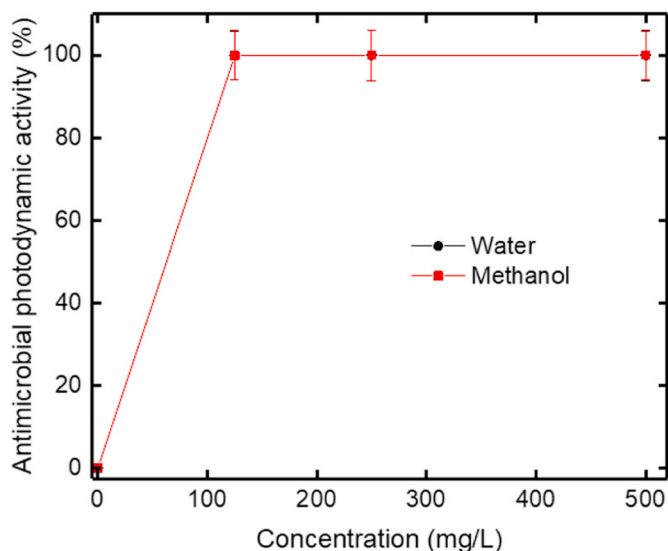


Fig. 13. Antimicrobial photodynamic activity in function of iron oxide nanoparticles concentration.

Fe<sub>3</sub>O<sub>4</sub> NPs from silky hairs boiled solutions (MH) and Chinese cabbage outer leaves (CCP). Both the MH derived FeO-NPs and CCP derived FeO-NPs exhibited antimicrobial activity against the *Candida* species and pathogenic bacteria. The reactive oxygen species produced by the FeO-NPs, including singlet oxygen (<sup>1</sup>O<sub>2</sub>), hydroxide radicals (OH•), and superoxide radicals (O<sup>2-</sup>), are thought to be the cause of microbial inhibition. ROS production has been discovered in a variety of metal oxide NPs, which could be the result of oxidative stress, inflammation, and subsequent damage to membranes, DNA, and proteins, which is one of the main mechanisms of nanotoxicity. It can be associated to a similar mechanism as the antimicrobial activity of newly synthesized green iron oxide nanoparticles.

### 3.6. Bacterial viability effect and antimicrobial photodynamic therapy

The influences of the different concentrations of synthesized nanoparticles on microbial cell viability were studied against *E. coli*. The results are represented in Figs. 10 and 11. At the concentrations of 125, 250 and 500 mg/L of FeO-NPs derived from water extract of plant, microbial cell viability inhibitions of *E. coli* were 93.24%, 96.31%, and 99.98%, respectively. While the iron oxide nanoparticles derived from methanol extract of plant inhibited the *E. coli* cell viability percentages were 91.87%, 95.09%, and 99.92% at 125, 250, and 500 mg/L, respectively. The mode of action of metallic NPs demonstrated the vigorous affinity of NPs against cell membranes of microorganisms. This is due to metallic NPs act as potent reductants and induce dissociation of functional groups in cell membrane liposaccharides and proteins. They can be oxidized by intracellular oxygen and induced oxidative harm through the Fenton reaction. The NPs penetration throughout the cell membrane creates physical detriment and causes to the pathogen microorganisms' death (Lee et al., 2008). Similar antimicrobial mechanism may be exhibited by both iron oxide nanoparticles synthesized in this research study. In addition, antimicrobial photodynamic therapy activity was investigated as well using LED irradiation. The results are represented in Figs. 12 and 13. As seen in Fig. 13, it was determined that strong antimicrobial photodynamic therapy activity was achieved with both synthesized FeO-NPs. Both green synthesized FeONPs inhibited the *E. coli* cell viability as 99.99%, 100% and 100% at 125, 250, and 500 mg/L, respectively. Podporska-Carroll et al. (2017) pointed out that the antimicrobial photodynamic therapy activity of fluorinated ZnO-NPs against *S. aureus* and *E. coli*. It was found that ZnO-NPs demonstrated 99.99% and 99.87% antibacterial activity against *S. aureus* and *E. coli*, respectively, after visible light irradiation. Sethi and Sakthivel (2017) defined the antimicrobial and antimicrobial photodynamic therapy activity of ZnO/TiO<sub>2</sub> nanocomposites against *E. coli*. It was found the ZnO/TiO<sub>2</sub> nanocomposite known higher *E. coli* growth inhibition under light irradiation than the ZnO or TiO<sub>2</sub> NPs without light irradiation. Magnetic nanoparticles (MNPs, Fe<sub>3</sub>O<sub>4</sub>), having a peroxidase-like activity, can be functionalized by conjugatively connecting photosensitizers

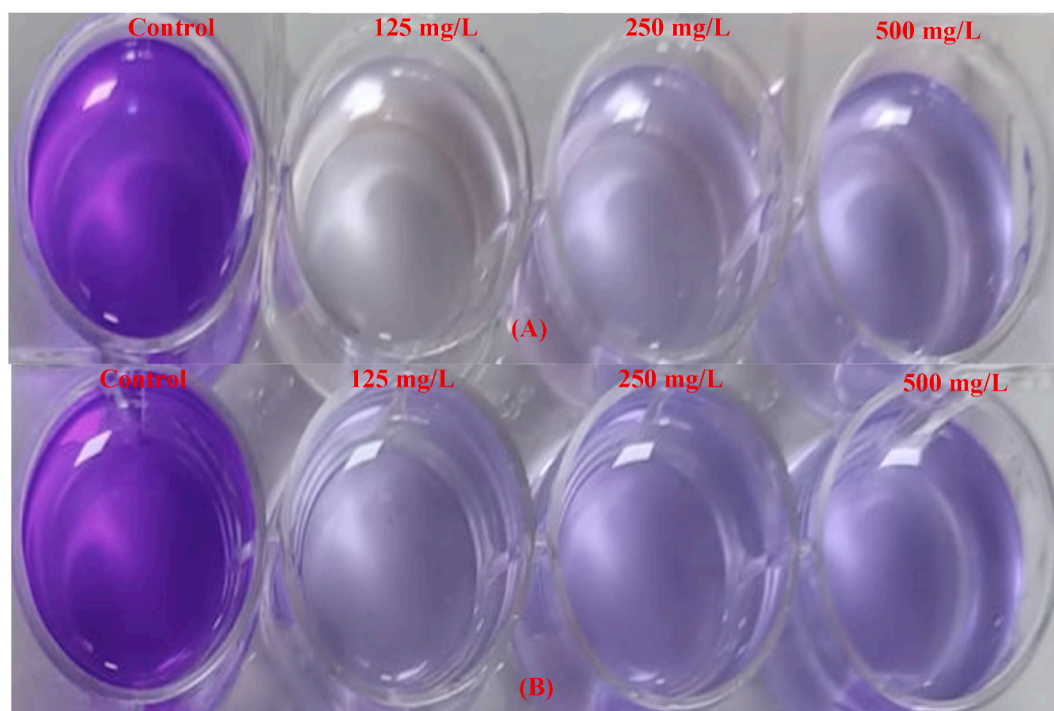
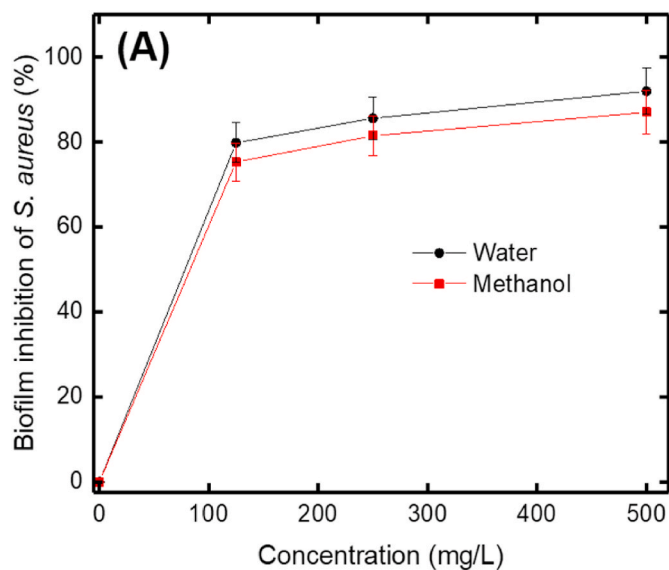


Fig. 14. Biofilm inhibition cells of green iron oxide nanoparticles using *S. aureus* in function of FeO-NPs concentration derived from (A) water extract and (B) methanol extract. (For interpretation of the references to color in this figure legend, the reader is referred to the Web version of this article.)



**Fig. 15.** Biofilm inhibition of green iron oxide nanoparticles using *S. aureus*. (For interpretation of the references to color in this figure legend, the reader is referred to the Web version of this article.)

and other molecules to its surface to increase the ROS generation at the targeted sites for antimicrobial photodynamic therapy usages (Tassa et al., 2011; Gao et al., 2014). According to these results, green synthesized FeO-NPs can be used as photosensitizers in antimicrobial photodynamic therapy activities.

### 3.7. Biofilm inhibition

A biofilm is a combination of surface-associated microbial cells surrounded in an extracellular polymeric material which is mainly a polysaccharide matrix, excreted by microbial cells. Microbial cells

secreted an extracellular polymeric substance which is mostly composed of polysaccharide matrix which is called a biofilm. This biofilm layer is a surface-associated microorganisms' assembly. Biofilms might form on an extensive kind of surfaces, including industrial or potable water system pipes, aquatic systems, medical devices or living tissues. *S. aureus*, *P. aeruginosa*, and *E. coli*, and *C. albicans* are well-known biofilm-producing microorganisms (Lebeaux et al., 2014). Biofilm causes an increase in antibiotic resistance. Therefore, biofilm-associated infections require specific antibiotic selection, high-dose administration, and long-term treatment processes. Ultimately, there is a need for new and more effective therapeutics (Girish et al., 2019). In this research study, the impact of synthesized FeO-NPs on biofilm inhibition

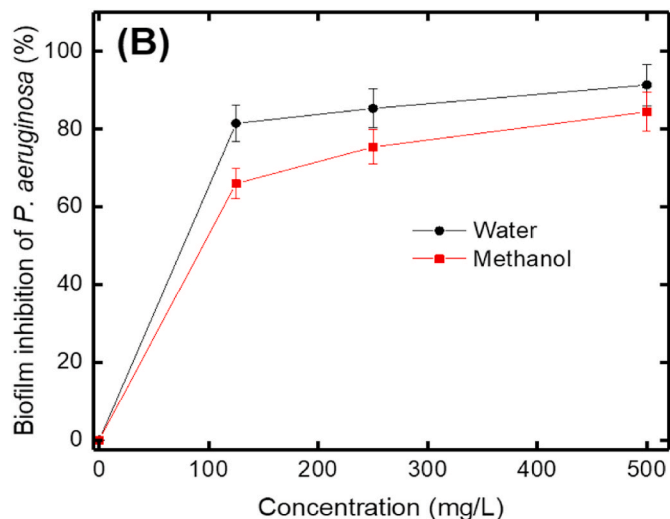


**Fig. 17.** Biofilm inhibition of green iron oxide nanoparticles using *P. aeruginosa*. (For interpretation of the references to color in this figure legend, the reader is referred to the Web version of this article.)

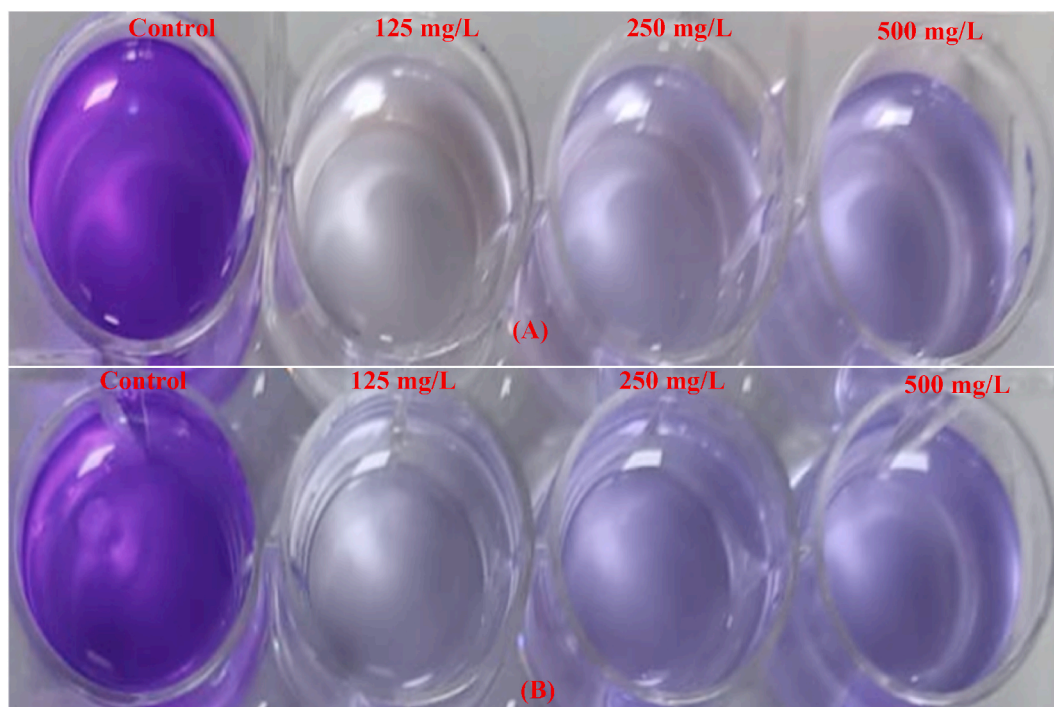


**Fig. 16.** Biofilm inhibition cells of green iron oxide nanoparticles using *P. aeruginosa* in function of FeO-NPs concentration derived from (A) water extract and (B) methanol extract. (For interpretation of the references to color in this figure legend, the reader is referred to the Web version of this article.)

was tested against *S. aureus* and *P. aeruginosa*. The results of the effect of FeO-NPs on the biofilm inhibitions of *S. aureus* and *P. aeruginosa* are illustrated in Figs. 14–17. As the concentration of the water extract of FeO-NPs augmented from 125 mg/L to 250 mg/L, the biofilm inhibitions of *S. aureus* and *P. aeruginosa* improved from 79.81% to 85.58% and from 81.44% to 85.29%, respectively (Figs. 15 and 17). On the other hand, when the concentration of the methanol extract of iron oxide nanoparticles raised from 125 mg/L to 250 mg/L, the biofilm inhibitions of *S. aureus* and *P. aeruginosa* increased from 75.29% to 81.45% and from 65.96% to 75.39%, respectively. The biofilm inhibition activity of the different nanoparticles has been studied by several researchers. A study established by Shahmoradi et al. (2021) has shown the effect of selenium nanoparticles on the biofilm inhibition in which a significant biofilm inhibition was observed. Bharathi et al. (2020) stated that the synthesized silver nanoparticle using *Cordia dichotoma* extract demonstrated dose-dependent biofilm inhibition activity against *S. aureus* and *E. coli* at the concentration ranges of 25–100 mg/L. Singh et al. (2018) stated that the Ag-NPs and Au-NPs derived from *Rhodiola rosea* rhizome extract were used against *P. aeruginosa* and *E. coli* for biofilm inhibition and both green synthesized nanoparticles displayed biofilm inhibition ability. According to the results of biofilm inhibition studies, newly synthesized and characterized iron oxide nanoparticles can be used for biofilm inhibition for different purposes.

To better understand the efficacy of our nanoparticles in removing contaminants as well as antimicrobial and antioxidant applications, we compared our findings to those of previous studies on similar iron nanoparticles, which are listed in Table 2. The obtained iron oxide nanoparticles were found to be more efficient in both dye removal and antibacterial and antioxidant applications.

#### 4. Conclusion

The two synthesized nanoparticles from Cs plant extracts were characterized and SEM demonstrated better uniform spherical morphology, which were used in Fenton reaction investigation for RR180 and BR18 dyes removal. The study showed complete elimination for both tested dyes in the optimized operating.

The DPPH scavenging activity results revealed that the green synthesized iron oxide nanoparticles exhibited an excellent radical scavenging ability. Both synthesized nanoparticles have also displayed good antibacterial activity, which inhibited the growth of Gram-negative, Gram-positive bacteria and micro fungus. From the obtained results of biofilm inhibition assay, the synthesized iron oxide nanoparticles exhibited high degree of biofilm inhibition ability at the different tested concentrations against *S. aureus* and *P. aeruginosa*. In addition, the new synthesized iron oxide nanoparticles demonstrated perfect antimicrobial photodynamic therapy and microbial cell viability inhibition against *E. coli*. The results obtained from this investigation may be beneficial for antimicrobial studies and preventing apoptotic cell proliferation.

#### Declaration of competing interest

The authors declare that they have no known competing financial interests or personal relationships that could have appeared to influence the work reported in this paper.

#### Data availability

No data was used for the research described in the article.

#### References

Abdullah, J.A.A., Salah Eddine, L., Abderrhmane, B., Alonso-González, M., Guerrero, A., Romero, A., 2020. Green synthesis and characterization of iron oxide nanoparticles by phenolic dactylifera leaf extract and evaluation of their antioxidant activity. *Sustain Chem Pharm* 17. <https://doi.org/10.1016/j.scp.2020.100280>.

Ağırtaş, S.M., Karataş, C., Özdemir, S., 2015. Synthesis of some metallophthalocyanines with dimethyl 5-(phenoxy)- isophthalate substituents and evaluation of their antioxidant-antibacterial activities. *Spectrochim. Acta Part A Mol Biomol Spectrosc* 135, 20–24. <https://doi.org/10.1016/j.saa.2014.06.139>.

Al-Asfar, A., Zaheer, Z., Aazam, E.S., 2018. Eco-friendly green synthesis of Ag@Fe bimetallic nanoparticles: antioxidant, antimicrobial and photocatalytic degradation of bromothymol blue. *J. Photochem. Photobiol. B Biol.* 185, 143–152. <https://doi.org/10.1016/j.jphotobiol.2018.05.028>.

Alavi-Tabari, S.A.R., Khalilzadeh, M.A., Karimi-Maleh, H., 2018. Simultaneous determination of doxorubicin and dasatinib as two breast anticancer drugs uses an amplified sensor with ionic liquid and ZnO nanoparticle. *J. Electroanal. Chem.* 811, 84–88. <https://doi.org/10.1016/j.jelechem.2018.01.034>.

Alper, M., Güneş, H., 2019. The anticancer and anti-inflammatory effects of Centaurea solstitialis extract on human cancer cell lines. *Turkish J Pharm Sci* 16, 273–281. <https://doi.org/10.4274/tjps.galenos.2018.27146>.

Alper, M., Özay, C., Güneş, H., Mammadov, R., 2021. Assessment of antioxidant and cytotoxic activities and identification of phenolic compounds of Centaurea solstitialis and urospermum picroides from Turkey. *Braz. Arch. Biol. Technol.* 64, 1–12. <https://doi.org/10.1590/1678-4324-2021190530>.

Antonoglou, O., Lafazanis, K., Mourdikoudis, S., Vourlias, G., Lialiaris, T., Pantazaki, A., et al., 2019. Biological relevance of CuFeO<sub>2</sub> nanoparticles: antibacterial and anti-inflammatory activity, genotoxicity, DNA and protein interactions. *Mater. Sci. Eng. C* 99, 264–274. <https://doi.org/10.1016/j.msec.2019.01.112>.

Ashraf, I., Singh, N.B., Agarwal, A., 2022. Green synthesis of iron oxide nanoparticles using Amla seed for methylene blue dye removal from water. *Mater. Today Proc.* <https://doi.org/10.1016/j.matpr.2022.07.404>.

Bautista, P., Mohedano, A.F., Gilarranz, M.A., Casas, J.A., Rodriguez, J.J., 2007. Application of Fenton oxidation to cosmetic wastewaters treatment. *J. Hazard Mater.* 143, 128–134. <https://doi.org/10.1016/j.jhazmat.2006.09.004>.

Baycan, N., Can, B., 2019. Color removal from yeast production industry wastewater using photo-fenton process. *Pamukkale Univ J Eng Sci* 25, 292–296. <https://doi.org/10.5505/pajes.2018.78872>.

Behin, J., Akbari, A., Mahmoudi, M., Khajeh, M., 2017. Sodium hypochlorite as an alternative to hydrogen peroxide in Fenton process for industrial scale. *Water Res.* 121, 120–128. <https://doi.org/10.1016/j.watres.2017.05.015>.

Bharathi, D., Vasantharaj, S., Bhuvaneshwari, V., 2020. Green synthesis of silver nanoparticles using *Cordia dichotoma* fruit extract and its enhanced antibacterial, anti-biofilm and photo catalytic activity. *J Phys Energy* 2. <https://doi.org/10.1088/2053-1591/aac2ef>, 0–31.

Bhuyar, P., Rahim, M.H.A., Sundararaju, S., Ramaraj, R., Maniam, G.P., Govindan, N., 2020. Synthesis of silver nanoparticles using marine macroalgae *Padina* sp. and its antibacterial activity towards pathogenic bacteria. *Beni-Suef Univ J Basic Appl Sci* 9. <https://doi.org/10.1186/s43088-019-0031-y>.

Bouchareb, R., Derbal, K., Ozay, Y., Niboucha, C., Bouti, M., Bouchareb, E.M., et al., 2022. Application of nanotechnology in anaerobic digestion for biohydrogen production improvement from natural coagulation/flocculation sludge using metallic oxide nanoparticles. *Energy Sources, Part A Recover Util Environ Eff* 44, 8184–8197. <https://doi.org/10.1080/15567036.2022.2120931>.

Cai, Q.Q., Jothinathan, L., Deng, S.H., Ong, S.L., Ng, H.Y., Hu, J.Y., 2021. Fenton- and ozone-based AOP processes for industrial effluent treatment. <https://doi.org/10.1016/b978-0-12-821011-6.00011-6>.

Chavan, R.R., Bhinge, S.D., Bhutkar, M.A., Randive, D.S., Wadkar, G.H., Todkar, S.S., et al., 2020. Characterization, antioxidant, antimicrobial and cytotoxic activities of green synthesized silver and iron nanoparticles using alcoholic *Blumea eriantha* DC plant extract. *Mater. Today Commun.* 24, 101320. <https://doi.org/10.1016/j.mtcomm.2020.101320>.

Chen, S., Fang, A., Zhong, Y., Tang, J., 2022. Ziziphora clinopodioides Lam leaf aqueous extract mediated novel green synthesis of iron nanoparticles and its anti-hemolytic anemia potential: a chemobiological study. *Arab. J. Chem.* 15, 103561. <https://doi.org/10.1016/j.arabj.2021.103561>.

Dave, P.N., Chopda, L.V., 2014. Application of iron oxide nanomaterials for the removal of heavy metals. *J Nanotechnol* 2014. <https://doi.org/10.1155/2014/398569>.

De, A., Das, R., Kaur, H., Jain, P., 2022. Synthesis, physicochemical investigations, DNA cleavage activity of biogenic zinc oxide nanoparticles and their interaction with Calf Thymus DNA. *Mater. Today: Proc.* 49, 3260–3264. <https://doi.org/10.1016/j.matpr.2020.12.742>.

Deokar, G.K., Ingale, A.G., 2016. Green synthesis of gold nanoparticles (Elixir of Life) from banana fruit waste extract-an efficient multifunctional agent. *RSC Adv.* 6, 74620–74629. <https://doi.org/10.1039/c6ra14567a>.

Dreher, K.L., 2004. Health and environmental impact of nanotechnology: toxicological assessment of manufactured nanoparticles. *Toxicol. Sci.* 77, 3–5. <https://doi.org/10.1093/toxsci/kfh041>.

Dukes Js, R.C.N., Loarie, S.R., Field, C.B., 2013. Strong response of an invasive plant species (*Centaurea solstitialis* L.) to global environmental changes. *Ecol. Appl.* 23, 515–522.

Duman, F., Ocoy, I., Kup, F.O., 2016. Chamomile flower extract-directed CuO nanoparticle formation for its antioxidant and DNA cleavage properties. *Mater. Sci. Eng. C* 60, 333–338. <https://doi.org/10.1016/j.msec.2015.11.052>.

El-Desoky, H.S., Ghoneim, M.M., El-Sheikh, R., Zidan, N.M., 2010. Oxidation of Levafix CA reactive azo-dyes in industrial wastewater of textile dyeing by electro-generated Fenton's reagent. *J. Hazard Mater.* 175, 858–865. <https://doi.org/10.1016/j.jhazmat.2009.10.089>.

Ensafi, A.A., Taei, M., Khayamian, T., Karimi-Maleh, H., Hasanpour, F., 2010. Voltammetric measurement of trace amount of glutathione using multiwall carbon nanotubes as a sensor and chlorpromazine as a mediator. *J. Solid State Electrochem.* 14, 1415–1423. <https://doi.org/10.1007/s10008-009-0978-z>.

- Eskikaya, O., Gun, M., Bouchareb, R., Bilici, Z., et al., 2022. Photocatalytic activity of calcined chicken eggshells for Safranin and Reactive Red 180 decolorization. *Chemosphere* 304, 135210. <https://doi.org/10.1016/j.chemosphere.2022.135210>.
- Eskikaya, O., Ozdemir, S., Tollu, G., Dizge, N., et al., 2022. Synthesis of two different zinc oxide nanoflowers and comparison of antioxidant and photocatalytic activity. *Chemosphere* 306, 135389. <https://doi.org/10.1016/j.chemosphere.2022.135389>.
- Gao, L., Giglio, K.M., Nelson, J.L., Sondermann, H., Travis, A.J., 2014. Ferromagnetic nanoparticles with peroxidase-like activity enhance the cleavage of biological macromolecules for biofilm elimination. *Nanoscale* 6, 2588–2593. <https://doi.org/10.1039/c3nr05422e>.
- Getahun, Y.W., Gardea-Torresdey, J., Manciu, F.S., Li, X., El-Gendy, A.A., 2022. Green synthesized superparamagnetic iron oxide nanoparticles for water treatment with alternative recyclability. *J. Mol. Liq.* 356, 118983 <https://doi.org/10.1016/j.molliq.2022.118983>.
- Girish, V.M., Liang, H., Aguilan, J.T., Nosanchuk, J.D., Friedman, J.M., Nacharaju, P., 2019. Anti-biofilm activity of garlic extract loaded nanoparticles. *Nanomed. Nanotechnol. Biol. Med.* 20 <https://doi.org/10.1016/j.nano.2019.04.012>.
- Gonca, S., Arslan, H., Isik, Z., Özdemir, S., Dizge, N., 2021. The surface modification of ultrafiltration membrane with silver nanoparticles using *Verbascum thapsus* leaf extract using green synthesis phenomena. *Surface. Interfac.* 26 <https://doi.org/10.1016/j.surfin.2021.101291>.
- Gusain, R., Kumar, N., Ray, S.S., 2020. Recent advances in carbon nanomaterial-based adsorbents for water purification. *Coord. Chem. Rev.* 405, 213111 <https://doi.org/10.1016/j.ccr.2019.213111>.
- Haber, F., Weiss, J., 1932. Über die Katalyse des Hydroperoxydes. *Naturwissenschaften* 20, 948–950. <https://doi.org/10.1007/BF01504715>.
- Hierro, J.L., Eren, Ö., Khetsuriani, L., Diaconu, A., Török, K., Montesinos, D., et al., 2009. Germination responses of an invasive species in native and non-native ranges. *Oikos* 118, 529–538. <https://doi.org/10.1111/j.1600-0706.2008.17283.x>.
- Iqbal, J., Abbasi, B.A., Ahmad, R., Shahbaz, A., Zahra, S.A., Kanwal, S., et al., 2020. Biogenic synthesis of green and cost effective iron nanoparticles and evaluation of their potential biomedical properties. *J. Mol. Struct.* 1199 <https://doi.org/10.1016/j.jmolstruc.2019.126979>.
- Jadhav, P., Nasrullah, M., Zularisam, A.W., Bhuyar, P., Krishnan, S., Mishra, P., 2021. Direct interspecies electron transfer performance through nanoparticles (NPs) for biogas production in the anaerobic digestion process. *Int. J. Environ. Sci. Technol.* 19, 10427–10439. <https://doi.org/10.1007/s13762-021-03664-w>.
- Karaman, C., Karaman, O., Atar, N., Yola, M.L., 2021. Tailoring of cobalt phosphide anchored nitrogen and sulfur co-doped three dimensional graphene hybrid: boosted electrocatalytic performance towards hydrogen evolution reaction. *Electrochim. Acta* 380. <https://doi.org/10.1016/j.electacta.2021.138262>.
- Karimi-Maleh, H., Tahernejad-Javazmi, F., Daryanavard, M., Hadadzadeh, H., Ensaifi, A.A., Abbasghorbani, M., 2014. Electrochemical and simultaneous determination of ascorbic acid, nicotinamide adenine dinucleotide and folic acid at ruthenium(II) complex-ZnO/CNTs nanocomposite modified carbon paste electrode. *Electroanalysis* 26, 962–970. <https://doi.org/10.1002/elan.201400013>.
- Khan, R.A., Khan, N.A., Morabet, R.E., Alsubih, M., et al., 2023. Comparison of constructed wetland performance coupled with aeration and tubasettler for pharmaceutical compound removal from hospital wastewater. *Environ. Res.* 216, 114437. <https://doi.org/10.1016/j.envres.2022.114437>.
- Klahan, R., Yuangsoi, B., Whangchai, N., Ramaraj, R., et al., 2023. Biorefining and biotechnology prospects of low-cost fish feed on Red tilapia production with different feeding regime. *Chemosphere* 311, 137098. <https://doi.org/10.1016/j.chemosphere.2022.137098>.
- Kumar, B., Smita, K., Galeas, S., Sharma, V., Guerrero, V.H., Debut, A., et al., 2020. Characterization and application of biosynthesized iron oxide nanoparticles using *Charus paradisi* peel: a sustainable approach. *Inorg. Chem. Commun.* 119, 108116 <https://doi.org/10.1016/j.inoche.2020.108116>.
- Le, N.T., Dang, T.D., Hoang Binh, K., Nguyen, T.M., Xuan, T.N., La, D.D., et al., 2022. Green synthesis of highly stable zero-valent iron nanoparticles for organic dye treatment using *Cleistanthus operculatus* leaf extract. *Sustain Chem Pharm* 25, 100598. <https://doi.org/10.1016/j.scp.2022.100598>.
- Lebeaux, D., Ghigo, J.-M., Beloin, C., 2014. Biofilm-related infections: bridging the gap between clinical management and fundamental aspects of recalcitrance toward antibiotics. *Microbiol. Mol. Biol. Rev.* 78, 510–543. <https://doi.org/10.1128/mmb.00013-14>.
- Lee, Y., Lee, W., 2010. Degradation of trichloroethylene by Fe(II) chelated with cross-linked chitosan in a modified Fenton reaction. *J. Hazard Mater.* 178, 187–193. <https://doi.org/10.1016/j.jhazmat.2010.01.062>.
- Lee, C., Kim, J.E.E.Y., Lee, W. II, Nelson, K.L., Yoon, J., Sedlak, D.L., 2008. Bactericidal effect of zero-valent iron nanoparticles on *Escherichia coli*. *Environ. Sci. Technol.* 42, 4927–4933.
- Lu-Irving, P., Harenčár, J.G., Sounart, H., Welles, S.R., Swope, S.M., Baltrus, D.A., et al., 2019. Native and invading yellow starthistle (*Centaurea solstitialis*) microbiomes differ in composition and diversity of bacteria. *mSphere* 4. <https://doi.org/10.1128/msphere.00088-19>.
- Mirza, A.U., Kareem, A., Nami, S.A.A., Khan, M.S., Rehman, S., Bhat, S.A., et al., 2018. Biogenic synthesis of iron oxide nanoparticles using *Aegrewia optiva* and *Prunus persica* phyto species: characterization, antibacterial and antioxidant activity. *J. Photochem. Photobiol. B Biol.* 185, 262–274. <https://doi.org/10.1016/j.jphotobiol.2018.06.009>.
- Mishra, B., Ghosh, D., Tripathi, B.P., 2022. Finely dispersed AgPd bimetallic nanoparticles on a polydopamine modified metal organic framework for diverse catalytic applications. *J. Catal.* 411, 1–14. <https://doi.org/10.1016/j.jcat.2022.03.009>.
- Muzafar, W., Kanwal, T., Rehman, K., Perveen, S., Jabri, T., Qamar, F., et al., 2022. Green synthesis of iron oxide nanoparticles using *Melia azedarach* flowers extract and evaluation of their antimicrobial and antioxidant activities. *J. Mol. Struct.* 1269, 133824 <https://doi.org/10.1016/j.molstruc.2022.133824>.
- Pandey, S., Son, N., Kim, S., Balakrishnan, D., Kang, M., 2022. Locust Bean gum-based hydrogels embedded magnetic iron oxide nanoparticles nanocomposite: Advanced materials for environmental and energy applications. *Environ. Res.* 214, 114000. <https://doi.org/10.1016/j.envres.2022.114000>.
- Patra, J.K., Baek, K.H., 2017. Green biosynthesis of magnetic iron oxide (Fe<sub>3</sub>O<sub>4</sub>) nanoparticles using the aqueous extracts of food processing wastes under photocatalyzed condition and investigation of their antimicrobial and antioxidant activity. *J. Photochem. Photobiol. B Biol.* 173, 291–300. <https://doi.org/10.1016/j.jphotobiol.2017.05.045>.
- Pelosi, B.T., Lima, L.K.S., Vieira, M.G.A., 2014. Removal of the synthetic dye remazol brilliant blue r from textile industry wastewaters by biosorption on the macrophyte *Salvinia natans*. *Braz. J. Chem. Eng.* 31, 1035–1045. <https://doi.org/10.1590/0104-6632.20140314s00002568>.
- Podporska-Carroll, J., Myles, A., Quilty, B., McCormack, D.E., Fagan, R., Hinder, S.J., et al., 2017. Antibacterial properties of F-doped ZnO visible light photocatalyst. *J. Hazard Mater.* 324, 39–47. <https://doi.org/10.1016/j.jhazmat.2015.12.038>.
- Raji, M., Mirbagheri, S.A., Ye, F., Dutta, J., 2021. Nano zero-valent iron on activated carbon cloth support as Fenton-like catalyst for efficient color and COD removal from melanoidin wastewater. *Chemosphere* 263, 127945. <https://doi.org/10.1016/j.chemosphere.2020.127945>.
- Raouf, J.B., Ojani, R., Karimi-Maleh, H., Hajmohamadi, M.R., Biparva, P., 2011. Multi-wall carbon nanotubes as a sensor and ferrocene dicarboxylic acid as a mediator for voltammetric determination of glutathione in hemolysed erythrocyte. *Anal. Methods* 3, 2637–2643. <https://doi.org/10.1039/c1ay05031a>.
- Rostamizadeh, E., Iranbaksh, A., Majd, A., Arbabian, S., Mehregan, L., 2020. Green synthesis of Fe<sub>2</sub>O<sub>3</sub> nanoparticles using fruit extract of *Cornus mas* L. and its growth-promoting roles in Barley. *J. Nanostructure Chem* 10, 125–130. <https://doi.org/10.1007/s40097-020-00335-z>.
- Sandupatla, R., Dongamani, A., Koyyati, R., 2021. Antimicrobial and antioxidant activities of phytosynthesized Ag, Fe and bimetallic Fe-Ag nanoparticles using *Passiflora edulis*: a comparative study. *Mater. Today Proc.* 44, 2665–2673. <https://doi.org/10.1016/j.matpr.2020.12.679>.
- Sathishkumar, P., Arulkumar, M., Palvannan, T., 2012. Utilization of agro-industrial waste *Jatropha curcas* pods as an activated carbon for the adsorption of reactive dye Remazol Brilliant Blue R (RBBR). *J. Clean. Prod.* 22, 67–75. <https://doi.org/10.1016/j.jclepro.2011.09.017>.
- Sethi, D., Sakthivel, R., 2017. ZnO/TiO<sub>2</sub> composites for photocatalytic inactivation of *Escherichia coli*. *J. Photochem. Photobiol. B Biol.* 168, 117–123. <https://doi.org/10.1016/j.jphotobiol.2017.02.005>.
- Shahmoradi, S., Shariati, A., Zargar, N., Yadegari, Z., Asnaashari, M., Amini, S.M., et al., 2021. Antimicrobial effects of selenium nanoparticles in combination with photodynamic therapy against *Enterococcus faecalis* biofilm. *Photodiagnosis Photodyn. Ther.* 35, 102398. <https://doi.org/10.1016/j.pdpdt.2021.102398>.
- Sheldon, R.A., Kochi, J.K., 1976. Metal-Catalyzed oxidations of organic compounds in the liquid phase: a mechanistic approach. *Adv. Catal.* 25, 272–413. [https://doi.org/10.1016/S0360-0564\(08\)60316-8](https://doi.org/10.1016/S0360-0564(08)60316-8).
- Shen, Z., Wang, W., Jia, J., Ye, J., Feng, X., Peng, A., 2001. Degradation of dye solution by an activated carbon fiber electrode electrolysis system. *J. Hazard Mater.* 84, 107–116. [https://doi.org/10.1016/S0304-3894\(01\)00201-1](https://doi.org/10.1016/S0304-3894(01)00201-1).
- Singh, P., Pandit, S., Beshay, M., Mookapati, V.R.S.S., Garnaes, J., Olsson, M.E., et al., 2018. Anti-biofilm effects of gold and silver nanoparticles synthesized by the *Rhodiola rosea* rhizome extracts. *Artif. Cell Nanomed. Biotechnol.* 46, S886–S899. <https://doi.org/10.1080/21691401.2018.1518909>.
- Sudhakar, C., Poonkothai, M., Selvamkar, T., Selvam, K., Rajivgandhi, G., Siddiqi, M. Z., et al., 2021. Biomimetic synthesis of iron oxide nanoparticles using *Canthium coromandelicum* leaf extract and its antibacterial and catalytic degradation of Janus green. *Inorg. Chem. Commun.* 133, 108977. <https://doi.org/10.1016/j.inoche.2021.108977>.
- Taherkhani, A., Jamali, T., Hadadzadeh, H., Karimi-Maleh, H., Beitollahi, H., Taghavi, M., et al., 2014. ZnO nanoparticle-modified ionic liquid-carbon paste electrode for voltammetric determination of folic acid in food and pharmaceutical samples. *Ionics* 20, 421–429. <https://doi.org/10.1007/s11581-013-0992-0>.
- Tassa, C., Shaw, S.Y., Weissleder, R., 2011. Dextran-coated iron oxide nanoparticles: a versatile platform for targeted molecular imaging, molecular diagnostics, and therapy. *Acc. Chem. Res.* 44, 842–852. <https://doi.org/10.1021/ar200084x>.
- Vasseghian, Y., Arunkumar, P., Joo, S.W., Gnanasekaran, L., Kamyab, H., 2022. Metal-organic framework-enabled pesticides are an emerging tool for sustainable cleaner production and environmental hazard reduction. *J. Clean. Prod.* 373, 133966. <https://doi.org/10.1016/j.jclepro.2022.133966>.
- Velsankar, K., Parvathy, G., Mohandoss, S., Ravi, G., Sudhakar, S., 2022. Journal of Drug Delivery Science and Technology Echinocloa frumentacea grains extract mediated synthesis and characterization of iron oxide nanoparticles : a greener nano drug for potential biomedical applications. *J. Drug Deliv. Sci. Technol.* 76, 103799. <https://doi.org/10.1016/j.jddst.2022.103799>.
- Yang, H., Shi, B., Wang, S., 2018. Fe oxides loaded on carbon cloth by hydrothermal process as an effective and reusable heterogeneous Fenton catalyst. *Catalysts* 8. <https://doi.org/10.3390/catal8050207>.

- Yeşilada, E., Honda, G., Sezik, E., Tabata, M., Fujita, T., Tanaka, T., et al., 1995. Traditional medicine in Turkey. V. Folk medicine in the inner Taurus Mountains. *J. Ethnopharmacol.* **46**, 133–152. [https://doi.org/10.1016/0378-8741\(95\)01241-5](https://doi.org/10.1016/0378-8741(95)01241-5).
- Yilmaz, G., 2018. Some medicinal plants used as folk medicine for dermatological diseases in European Turkey. *Curr Perspect Med Aromat Plants* **1**, 48–52.
- Yoonus, J., Resmi, R., Beena, B., 2020. Evaluation of antibacterial and anticancer activity of green synthesized iron oxide ( $\alpha$ -Fe<sub>2</sub>O<sub>3</sub>) nanoparticles. *Mater. Today Proc.* **46**, 2969–2974. <https://doi.org/10.1016/j.matpr.2020.12.426>.